Semiconducting Phase in Borophene: Role of Defect & Strain

Semiconducting Phase in Borophene: Role of Defect & Strain

Gargee Bhattacharyya,[†] Arup Mahata,[#] Indrani Choudhuri,[#] Biswarup Pathak,[†,#,*]

[†] Discipline of Metallurgy Engineering and Materials Science, [#]Discipline of Chemistry, School of Basic Sciences and, Indian Institute of Technology (IIT) Indore, Indore, Madhya Pradesh, 453552, India
Email: biswarup@iiti.ac.in

Abstract:

Boron is an interesting element due to its chemical and structural complexity. Recent synthesis of borophene led scientists to study boron monolayer based materials for various applications. Using density functional theory (DFT) calculations, nineteen different phases of boron monolayer (with hexagonal hole-densities from 1/32 to 8/32) are studied to understand their origin of buckling, stability and planarity. Projected densities of states of various phases of borophene based systems with defect are plotted into in-plane ($s+p_x+p_y$) and out-of-plane (p_z) orbitals to understand the role of σ and π-bands towards their geometry and stability. Interestingly, λ_5-sheet shows semiconducting properties under uniaxial/biaxial tensile/compressive strains and the λ_5-sheet shows excellent dynamical, thermal and mechanical properties and thus a promising semiconducting phase for electronic devices.

Keywords: Borophene, Defect, Planar, Hexagonal hole density, Semiconductor

1. Introduction:

Research on two-dimensional (2D) atomic crystals has become one of the hottest topics in condensed matter physics and materials science for many years. The first successful realization of thermodynamically stable free-standing two-dimensional graphene with its outstanding electrical, optical and thermo-mechanical properties has given the breakthrough for the intense research on wide range of 2D materials. The distinct and excellent properties of graphene[1-5] make it as a promising material for diverse technological applications.[6-10] These fascinating properties of graphene trigger the scientists to explore other group III-V monolayer based systems. Over the past one decade silicene,[11] germanene,[12] stanene,[13] borophene,[14,15,16] phosphorene,[17] have been synthesized in the main group family.

Other than carbon, boron is the second element that can exhibit multiple forms of low-dimensional allotropic structures. This growing interest explores varieties of pure boron in the form of novel solids, quasiplanar clusters, nanosheets, nanotubes, nanoropes, nanospheres, nanowires, nanobelts, nanoribbons, and quasi-crystals.[18] These are best alternatives to carbon allotropes having superior or similar characteristics. Theoretical anticipation of the stability of boron nanotubes,[19] and the successful synthesis of multi-walled boron nanotubes (MWBNT)[20] instigates the possibility of formation of boron monolayer sheet because boron nanotubes can be made of rolling up the 2D boron sheet.

Unlike graphene and some other two dimensional materials, bulk 2D layered structure of boron is barely found in nature owing to atomic arrangements of boron in the lattice, which acts as a driving force to form generally more buckled and corrugated structures. This makes it challenging to mechanically exfoliate during experimental synthesis. As a result experimental synthesis of 2D boron monolayer can only be possible by thermal evaporation deposition; chemical vapor deposition or molecular beam epitaxy procedure.[21] Contemporary experimental researches demonstrate both the experimental synthesis of boron nanotube[19-20] and monolayer of boron on Ag (111) surface.[14]

However, defects are almost inevitable during the fabrication process such as mechanical exfoliation, chemical vapor deposition, ion or electron irradiation of two-dimensional materials and their existence strongly alter thermodynamic, mechanical and electronic properties of their pristine counterparts.[22-23] Inversely deliberate introduction of defects can be a possible approach to alter the properties of the pristine materials.[24,25,26] Recent theoretical study reported the stability and electronic structures of various crystalline buckled and unbuckled monolayer structures of boron, which include the α-sheet,[27] β-sheet,[27] γ-sheet,[18] g1/8- and g2/15-sheets and many more new boron sheets[28] with the presence of multi-vacancies in their structures. They have showed that all these boron sheets can be constructed by carving different patterns of hexagonal holes within the triangular sheet, and their area densities can be described by a global density parameter, η,[27] which is defined as the ratio of number of hexagon holes to the number of atomic sites in the pristine triangular sheet within a unit cell of the decorated boron sheet.[28] However, it has been found that most of the phases of borophene with uniform hole density are metallic in nature.[29,30] Very recently, Yakobson and co-workers showed a new dominion that 2D polymorph of boron can be superconductor.[31] These fascinating properties stimulate us to dig deep into the structure and properties of new phases of borophene based sheets specially with non-uniform distribution of holes.

However, major bottleneck preventing borophene from mainstream semiconductor industry is the lack of band gap. The lack of a finite band gap is a challenging obstacle for any material to use it in logic and high speed switching devices since current can never be turned off completely.[32] Various methods have been proposed through decades to open up the band gap in graphene or graphene like 2D materials.[33-37] Recently theoretical and experimental reports show that borophene and various phases of boron sheet can outperform some property of graphene which can be used as potential replacement of silicon in electronics industry. A recent theoretical study shows that alpha sheet is an indirect band gap semiconductor.[28] However, to the best of our knowledge; there are no other reports of semiconducting properties in borophene based systems.

Therefore in the present work, we have performed a systematic study to open up the band gap in borophene by creating defects. A series of various phases of borophene based sheets are studied for this. The stability, planarity, and electronic properties of these systems are studied to understand the role of defects. We have attempted to explain the stability and planarity of these different phases of borophene structure with defect from the total number of valance electrons and vacant σ and π bands. We have studied the effect of strain in the electronic properties of these systems as such systems are synthesized on a metallic substrate, which generates strain. At the end, the stability of the semiconducting borophene sheet has been evaluated from the energetic (cohesive energy), mechanical (stress vs strain relationship), dynamic (phonon dispersion) and thermal (molecular dynamics simulation) studies.

2. Computational Details:

The Vienna Ab initio Simulation Package (VASP)[38] is used to perform all the calculations. We have used the Perdew−Burke−Ernzerhof (PBE) exchange–correlation functional within the generalized gradient approximation (GGA)[39-40] for the accurate description of delocalized s and p electrons. Projected augmented wave (PAW) method[41] is employed using a 470 eV energy cut–off to describe the electronic wave function. The first Brillouin zone of borophene supercell (4×4×1) structure is sampled with a 9×15×1 Monkhorst−Pack K–point grid for geometry optimization and 13×23×1 for the electronic structure calculation. We have achieved self-consistency with the convergence tolerance set to 10^{-6} eV and 10^{-3} eV.$Å^{-1}$ for total energy and force calculations respectively.

A vacuum of 15 Å is employed along the z-direction to avoid any kind of interaction between the two periodic layers. Since its well-known that the DFT in GGA functional (such as PBE functional) tends to underestimate the band gap due to their inherent lack of derivative discontinuity[42] and the delocalization error.[43] So, the hybrid functional such as Heyd–Scuseria–Ernzerhof (HSE06)[44] is used to provide reasonable accurate electronic structure. A 3×5×1 Monkhorst−Pack K-point grid is used to perform HSE06 calculations. We have calculated the phonon properties using density functional perturbation theory (DFPT)[45] as implemented in the VASP and phonon dispersion calculations are carried out using

the Phonopy code.[46] The thermal stability of patterned borophene is verified by carrying out Ab Initio Molecular Dynamics simulations (AIMD) using a canonical ensemble at 300, 500 and 1000 K with a time step of 1 fs for 5 pico second (ps). The Nosé thermostat model [47] is used to control the temperature during the MD simulation.

Kresse and co-workers[48] reported that the phonon frequencies of bulk cubic diamond obtained with PBE are in reasonable agreement with experiment. In fact, they have reported that HSE increases the optical modes of phonon frequencies. Since boron is next to carbon (in the periodic table), we have used PBE functional for lattice dynamics. Furthermore, it is widely accepted in previous literatures[35,49] that PBE functional gives satisfactory result for AIMD simulation. Moreover, it will be computationally costly for doing AIMD simulation using hybrid calculations.

Energetic stability of the different phases of borophene structure with defect is investigated from the binding energy (eV) and the binding energy calculations are carried out using the following equation:[28]

$$E_B = E_{Boron} - E_{Defect} \quad (1)$$

Where E_{Boron} represents the total energy of a single boron atom and E_{Defect} is the total energy per boron atom of the different phases of borophene structure with defect . Binding energy refers to the energy required to isolate an atom from the system of several atoms. Therefore, we have considered the energy of single isolated boron atom while calculating the binding energy. Very recently, Karmodak et al.[50] defined the relative binding energy of free-standing borophene based systems as $E_1 = {}^1/_n\,(E_{Sheet} - nE_B)$ where E_{sheet} and E_B denote the energy of borophene sheet and energy of a single boron atom. Here, n is the number of boron atoms. Tang et al.[27,51] also calculated binding energy per atom of defected boron sheets using the same approach. The similar approach has been used in many cases previously.[18, 28, 49,52]

Relative binding energy per boron atom (E_{RB} in meV)[50] is calculated as the difference between the energy with respect to most energetically stable boron sheet which is α-boron sheet.

$$E_{RB} = [E_{Defect} - E_{\alpha-boron}] \quad (2)$$

Here, $E_{\alpha\text{-boron}}$ denotes the total energy (per boron atom) of α-boron sheet.

3. Results & Discussion:

3.1 Pure Borophene:

Obeying to Aufbau principle,[53] monolayer sheet of boron is a quasi-planar arrangement of hexagonal pyramidal B_7 units. A planar projection of this system forms a triangular lattice as shown in Figure 1a Boron monolayer sheet is constructed by adopting a buckled two atom orthorhombic unit cell with lattice parameters of a = 2.87 Å and b = 1.62 Å. Our calculated lattice parameters and the buckling height (h) of this sheet (0.91 Å) are found to be in good agreement with the previous theoretical report.[54] Figure 1b shows the total density of states and band structure of borophene unit cell calculated using HSE06 level of theory. We have calculated total/partial density of states and band structure of borophene unit cell using GGA PBE level of theory too (Figure S1, Supporting Information). We find our calculated results (GGA and HSE06) match with the earlier reports.[14,46] We have used HSE06 level of theory as it predicts electronic properties more accurately than the GGA PBE level of theory.[55] Thus, we have presented all our HSE06 results in our manuscript and GGA results in supporting information. The PDOS projections of in-plane (s+p_x+p_y) and out-of-plane (p_z) orbitals using HSE06 is presented in Figure 1c and GGA result is shown in Figure S1b (Supporting Information). The density of states of pure borophene unit cell shows that there are states at the Fermi energy level, which affirms that borophene is metallic. So, the lack of band gap and absence of planarity limits its devices based applications.[32]

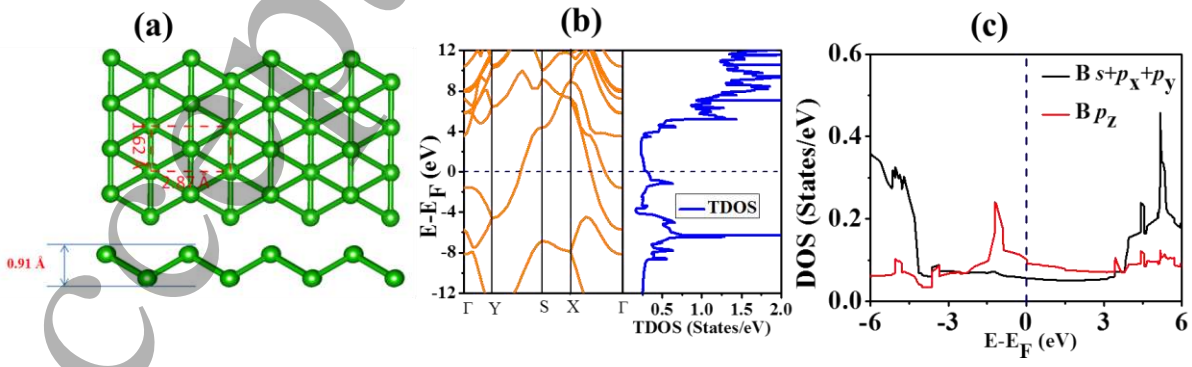

Figure 1: (a) Top and side views of borophene. The two-atom unit cell of borophene is indicated by the red dashed lines. (b) Band structure and density of states of borophene using HSE06 level of theory. (c) PDOS projections are onto in-plane (s+p_x+p_y) and out-of-plane (p_z) orbitals calculated by HSE06. The Fermi level is set to zero and indicated by the blue dashed line.

3.2. 2D phases/polymorph of borophene:

We have studied the various 2D phases of boron with a different extent of vacancy to understand their importance in electronic and optoelectronic properties. These sheets are constructed from a (4×4×1) borophene supercell structure consisting of 32 boron atoms. Although there are other possibilities of making a supercell of 32 atoms with hexagonal cell, we have chosen orthorhombic unit cell since most of the previous reports[14,29] other than α-boron sheet contains orthorhombic cell and it is logical to make orthorhombic supercell of 32 atoms since borophene unit cell is orthorhombic.[14] Different phases of borophenes have been modeled by maintaining different patterns of hexagonal holes within the triangular sheet. Besides, the area densities of the phases of borophenes based sheets have been described by a global density parameter as hexagonal hole-density (η).[27]

In the present work, we have created new phases of boron sheets with different hexagonal hole-density (η = 1/32 to 8/32) ranging from single vacancy to eight vacancies as depicted in Figure 2-4. Since most of the borophene phases with uniform hexagonal hole density are found to be metallic, we tried to investigate the situation whether non-uniform distribution of holes can create a gap or very low density near the Fermi level. We have classified various phases of boron monolayer sheets in terms of the total coordination number (CN) present in the system:[28] (1) α-type (CN = 5, 6), (2) β-type (CN = 4, 5, 6), (3) λ-type (CN = 3, 4, 5, 6), (4) Ψ-type (CN = 3,4,5), (5) ζ-type (CN = 2,4,5,6) and (6) δ-type. The δ-type has a single CN value. The subscript of δ denotes the CN value of that particular δ structure (Table 1). We have compared the energetic stabilities of these sheets form their binding energy values (Table 1).[28] The electronic structures of these phases of borophene sheets have been compared with the pure borophene,

alpha and beta sheet (Figure 1, Figure S1, S5 and S6, Supporting Information). Besides, the bonding between in-plane and out-of-plane boron atoms has been discussed through the overlap between in-plane (sum of s, p_x and p_y) and out-of-plane (sum of p_z) orbitals. In case of borophene, the overlap is maximum between in-plane and out-of-plane states, which in turn stabilizes the buckling pattern in borophene.[27] The in-plane and out of-plane orbitals of buckled structures undergo orbital overlap. This orbital overlap basically helps the structure to be stable in buckled form. Tang et al.[27,51] also mentioned that the buckling pattern in triangular sheet can helps to mix the in plane and out of plane states and can be thought as a symmetry reducing distortion that eventually enhances binding.

Table 1: Binding energies (E_B), relative binding energies (E_{RB}), buckling height (h), coordination number (CN), and hexagonal hole-density (η) of pure and various phases of borophene based sheets.

S. No.	Sheet-type	h (Å)	CN	η	E_B (eV)	E_{RB} (meV)
1	δ_6 [14]	0.91	6	0	5.79	90
2	α_1	1.04	5,6	1/32 (0.03)	5.79	90
3	β_1	1.07	4,5,6	2/32 (0.06)	5.80	80
4	α_2	0.88	5,6	2/32 (0.06)	5.80	80
5	β_2	0.71	4,5,6	3/32 (0.09)	5.81	70
6	λ_1	1.01	3,4,5,6	3/32 (0.09)	5.79	90
7	α_3	0.85	5,6	3/32 (0.09)	5.84	40
8	α [27,28]	0.34	5,6	1/9 (0.11)	5.88	0
9	λ_2	0.74	3,4,5,6	4/32 (0.13)	5.80	80
10	β_3	0.83	4,5,6	4/32 (0.13)	5.66	220
11	β_4	1.02	4,5,6	4/32 (0.13)	5.75	130
12	β [27,28]	0.39	4,5,6	1/7 (0.14)	5.87	10
13	β_5	0.18	4,5,6	5/32 (0.16)	5.73	150
14	λ_3	1.58	3,4,5,6	6/32 (0.19)	5.65	230
15	λ_4	0.88	3,4,5,6	6/32 (0.19)	5.63	250
16	Ψ_1	0.06	3,4,5	7/32 (0.22)	5.70	180
17	ζ	0.28	2,4,5,6	7/32 (0.22)	5.71	170

18	δ_4 [28]	0.02	4	8/32 (0.25)	5.68	200
19	λ_5	0.71	3,4,5,6	8/32 (0.25)	5.52	360
20	β_6	0.16	4,5,6	8/32 (0.25)	5.73	150

Based on CN values[28], we have listed a total of twenty borophene based structures. We have studied a total of 19 borophene based structures with defects in the manuscript. However, three structures (alpha, beta and λ_4 structures) have been reported in the literature. Therefore, in this manuscript, we have proposed 16 new structures. For comparisons, we have studied these three previously reported structures

Our binding energy values show that α-sheet with η=1/9 is the most stable one (Table 1). This is very much in agreement with the earlier reports.[27,28] However, it is interesting to know that one of the phase of borophene sheet with defect (α-sheet) is the most stable compared to pure borophene (Table 1). On the other hand, λ_5 is the least stable with η=8/32. This indicates that structure with higher or lower hole density than 1/9 is a high energy phase structure. Also, structures with same hole density can have low to high energy phase structures (Table 1). Thus, the distribution of hexagonal holes is important for their stability. Likewise, the buckling/planarity of the structure depend on the distribution of hexagonal holes. Tang and Ismail-Beigi formulated based on their observation that planner boron sheet can be found with the hexagonal hole density in the range between $1/9 < \eta < 1/5$, where holes are evenly distributed all over the sheet.[51] It is also reported that planner boron sheet can be generated on the basis of evenly distribution of hexagonal hole in the triangular lattice.[51] Surprisingly, some of our predicted non-planar structures fall in the hexagonal hole density range of $1/9 < \eta < 1/5$.[51] The main reason behind such anomalous buckling is the non-uniform hole density distribution. Furthermore, we have found that some structures are very much planar with $\eta > 1/5$. Therefore, it will be interesting to find out the underlying reason behind such structures. To understand the buckling/planarity of different phases of borophene based structures, we have carefully investigated the contribution of filled/unfilled σ and π-bands to understand their geometry.

Tang and coworkers reported that there is an excess of electrons occupying the anti-bonding states and vacant bonding states in borophene which induces instability in the system.[27] As a result, the structure

buckles to improve the interaction between bonding and anti-bonding states. Therefore different phases of borophene structure with defect can be stable if we can remove the excess electrons from anti-bonding states. This is what happens with η=1/9, where total number electrons justify the electronic requirements in borophene.[50] Recently, Jemmis and coworkers explained the electronic requirement in borophene and made a vis-à-vis relation with MgB_2 in terms of total number of electrons.[50] Interestingly, they found that the different phases of borophene structure with defect are most stable while on the Ag substrate. More importantly, they demonstrated that structure with maximum hole density (η=1/5) is most stable over Ag-substrate. As we all know, such borophene monolayer based systems have been synthesized over a substrate and thus it is important to study structures with different hexagonal hole-densities for their synthesis and applications. Hence, we have discussed the electronic structures of the various different phases of borophene based sheets (η=1/32 to 8/32) and discussed their stability with respect to pure borophene.

3.2.1 Mono (η=1/32) and Bi (η=2/32) Vacancy in Borophene:

We have created a hexagonal hole in the 32-atomic borophene supercell, which corresponds to α_1 structure (Figure 2a). Similarly, we have created two vacancies to generate β_1 and α_2 phases as shown in figure 2b-c. The optimized structures show buckling height of 1.04 Å, 1.07 Å and 0.88 Å for α_1, β_1, and α_2 phases respectively. Tang and Ismail-Beigi predicted that the global density parameter (η) of buckled structures generally does not fall in the range between $1/9 < \eta < 1/5$.[51] Our modeled mono and bi vacancy structures follow the same trend as predicted by Tang and Ismail-Beigi.[51] However, the α_2 structure is more planar than β_1 sheet because the vacancy is uniformly distributed in α_2 structure. Our calculated density of states using HSE06 (Figure 2) and GGA-PBE (Figure S2, Supporting Information) level of theory shows that the structures are metallic. In case of α_1, there is an excess of electrons in the out-of-plane (p_z) anti-bonding orbitals. For β_1, there is an excess of electrons in both in-plane and out-of-plane anti-bonding orbitals. Such filled anti-bonding orbitals lead to buckling. In comparison to MgB_2, borophene can be seen as $B\text{-}B_2$, where each carbon atom is replaced by boron atom in the graphene

structure and one extra boron atom is placed in the middle of the hexagon. Karmodak et al.[50] discussed that when there is an excess of electron in the anti-bonding orbitals, the system became destabilized. This destabilization is reduced by non-planner distortion. However in the case of α_2, both in-plane and out-of-plane bonding orbitals are filled close to the Fermi level and thus the structure is more planar over the other two structures.

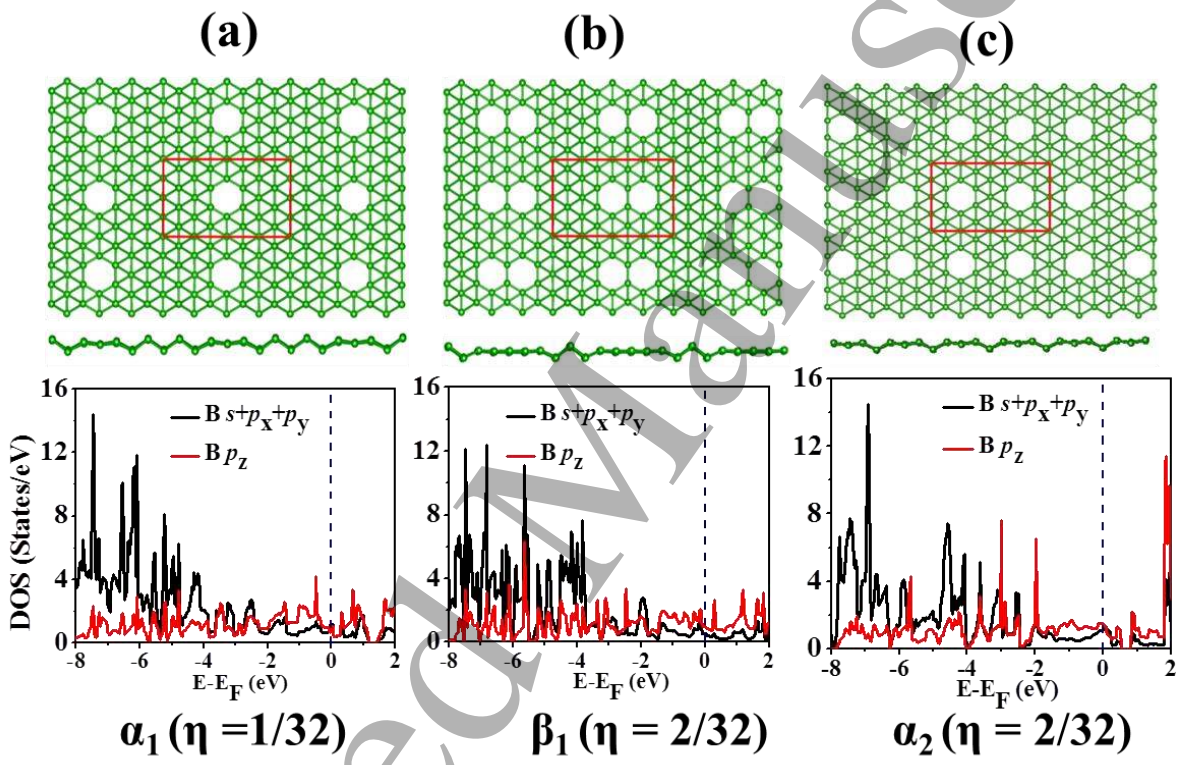

Figure 2: Structure and partial density (using HSE06) of states of (a) α_1, (b) β_1 and (c) α_2 phase. The red rectangle denotes the supercell of different phases of borophene based sheet and the Fermi level is set to zero and indicated by the blue dashed line.

3.2.2 Tri (3/32), Tetra (4/32) and Penta (5/32) Vacancy in Borophene:

Figure 3 shows tri, tetra, and penta vacancy borophene structures. Three stable phases (β_2, λ_1 and α_3) are identified with η=3/32. Similarly, three more stable phases (λ_2, β_3 and β_4) are predicted for η=4/32 and one stable structure with η=5/32. The calculated binding energy values (Table 1) are 5.81, 5.79, 5.84,

5.80, 5.66, 5.75, 5.73 eV/atom for β_2, λ_1, α_3, λ_2, β_3, β_4 and β_5 respectively. However, all the structures are buckled except β_5, which is almost planar. Interestingly, we find that the global density parameter of β_5 structure (η=5/32) falls in the range between $1/9 < \eta < 1/5$.[51] Therefore, in case of β_5, evenly distributed hole density parameter can successfully predict the planarity. In other cases, it is extremely difficult to explain the planarity/buckling of the structure based on the filled/vacant σ and π bands. Furthermore, it is extremely difficult to explain based on filled/vacant σ and π bands when holes are not evenly distributed. In such cases, a part of the structure is planar, whereas other part is buckled (Figure S3, Supporting Information). For this, we find a mixed pattern in terms of σ and π band stabilization and destabilization. Therefore, the stabilization of σ and π bands depends a lot on the pattern of hole distribution.

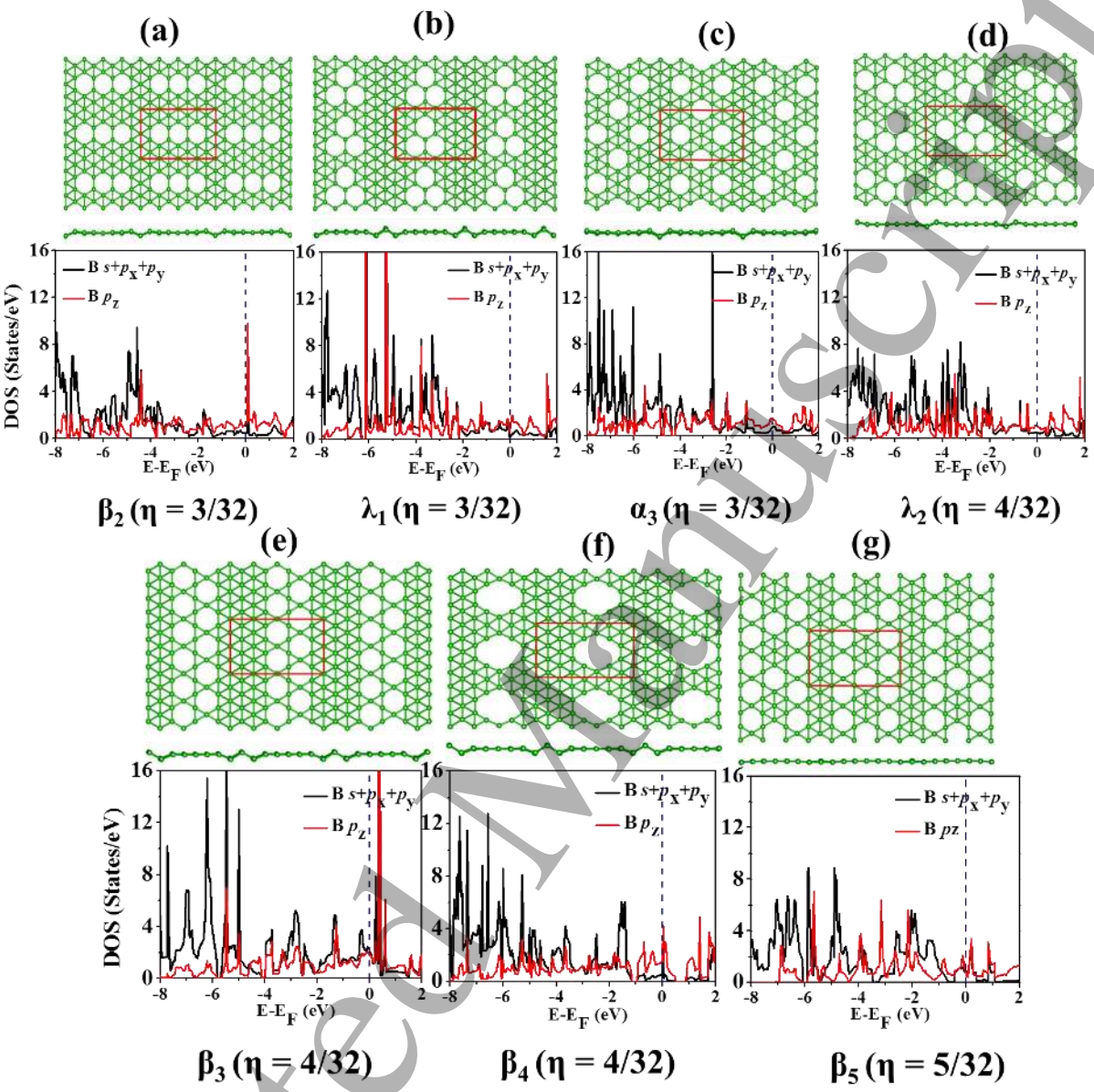

Figure 3: Structure and partial density (using HSE06) of states of (a) β_2, (b) λ_1, (c) α_3, (d) λ_2, (e) β_3, (f) β_4, and (g) β_5 phase. The red solid rectangle denotes the supercell of different phases of borophene based sheet and the Fermi level is set to zero and indicated by blue dashed line.

3.2.3 Hexa (6/32), Hepta (7/32) and Octa (8/32) Vacancy in Borophene:

Furthermore, various phases of 2D boron sheets with hole density from 6/32 to 8/32 are depicted in Figure 4a-g. The λ_3 and λ_4 structures with η=6/32, ψ_1 and ζ structures with η=7/32 and δ_4, λ_5 and β_6 with η=8/32 have been studied for this. The calculated cohesive energies are 5.65, 5.63, 5.70, 5.71, 5.68, 5.52 and 5.73 eV/atom for λ_3, λ_4, ψ_1, ζ, δ_4, λ_5 and β_6 structures, respectively. We find that ψ_1, δ_4, and β_6 structures (Figure 4c, 4e, and 4g, Figure S4, Supporting Information) are completely planar. Surprisingly, the hole density of these structure does not fall in the range of $1/9 < \eta < 1/5$. However, only δ_4 has uniform hole distribution, whereas other structures have non-uniform distribution of holes. In case of non-uniform distribution of holes, buckling analysis cannot be done comparing α sheet (which has uniform hole distribution) because buckling is not uniform all over the sheet. Some portion where holes are not present buckling is present and the sheet became planner where there are holes. It is extremely difficult to explain the planarity/buckling of the structure based on the filled/vacant σ and π bands since structures are neither perfectly planar nor buckled. Hence, we find a mixed pattern in terms of σ and π band stabilization and destabilization in their PDOS (Figure 4) plot. We have found that the δ_4 sheet is almost planner (buckling height ~ 0.02 Å) due to uniform distribution of holes. Other sheets such as ψ_1, ζ and β_6 which are closely planner (buckling height ~ 0.06 Å, 0.28 Å and 0.16 Å respectively) have non-uniform distribution of holes. It is also evident from the three phases with non-uniform distribution of holes that in plane states are zero thus no mixing between in plane and out-of-plane states near the Fermi level. Hence, we propose that hole density parameter is no longer universal for explaining the planarity for non-uniform vacancy structures. More importantly, a planar system with semiconducting nature may not be achieved due to the presence of density at the Fermi level.

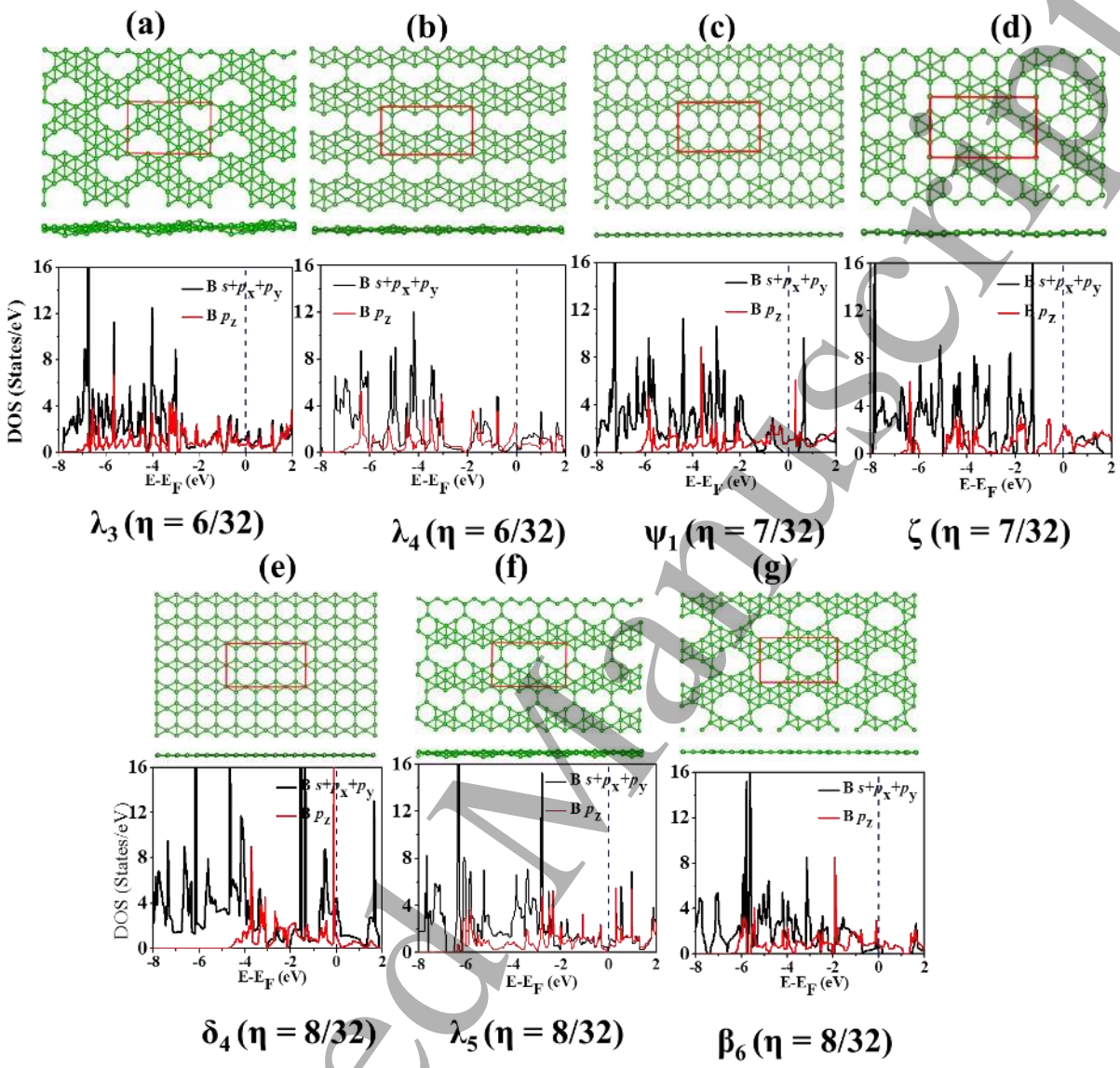

Figure 4: Structure and partial density (using HSE06) of states of (a) λ_3, (b) λ_4, (c) ψ_1, (d) ζ, (e) δ_4, (f) λ_5 and (g) β_6 phase. The red solid line rectangle denotes supercell of different phases of borophene based sheet and the Fermi level is set to zero and indicated by blue dashed line.

3.3. Energy Balance Position vs. Stability:

Ideally, while comparing with carbon, boron lacks one electron and cannot form a stable honeycomb like graphene structure; rather forms a triangular lattice in its two-dimensional structure. This two-dimensional triangular lattice based boron sheet is without any hexagonal hole (η = 0) and thus excess

electron makes the sheet buckled. On the contrary, the boron hexagonal honeycomb lattice[27] has the largest hexagonal hole density ($\eta = 1/3$), which is the most electron-deficient amongst the all the phases of borophene structures. This kind of electron deficiency contributes towards the stability of boron monolayer and can be nicely explained from the energy position of in-plane and out-of-plane bonding and anti-bonding states with respect to electron balance position. The electron energy balance position is considered as the position where the in-plane and out-of-plane electron occupation becomes zero or very less.[56] Therefore, the ideal boron monolayer should contain the hexagonal and triangular proportion in such a way that their Fermi position remains at the energy balance position of in-plane bonding and anti-bonding states so that all the in-plane bonding states becomes fully occupied and all of the anti-bonding states remains unoccupied. In fact, we have presented the DOS of α and β-boron sheet in the Figure S5 and S6, (Supporting Information) and it is found that electron balance position remain at the Fermi level. Hence, the bonding states of the systems are filled and the anti-bonding states of the systems are empty which indicates the maximum stability of the system. Therefore, comparing with α- sheet and β-sheet, we can predict that the λ_5 sheet (Figure 4f) is very promising compared to other proposed structures because the boundary position or the electron balance position between the bonding and anti-bonding states coincides with the Fermi level position which indicates that the in-plane bonding states are filled and anti-bonding states are empty resulting a perfect electron balance system. In fact, previous reports suggested that hybridization of triangular and hexagonal motifs in two dimensions can yield more stable and planner boron monolayer in some cases due to transfer of excess electrons from triangular lattice to the electron-deficient hexagonal lattice.[27] Therefore, we find that electron balance position can exist even in high energy structures also, which is very much different from the behavior of alpha and beta sheet. Hence, we believe that the presence of lower coordination number (CN = 3) makes the λ_5 sheet as a high energy structure.

We have investigated a total of 19 phases of borophene based systems with defect. Out of these 19 structures, three structures (alpha, beta and λ_4 structures) have been modeled as per the previously reported structures. Therefore in this manuscript, we have reported a total of 16 new phases of borophene

based structures and for comparisons, we have studied those three previously reported structures (alpha, beta and λ_4 structures). In all the previous reports, they have created patterned defects to get various phases of borophene based structures. However, we believe that in this process, we may miss some low energy structures having same hexagonal hole density. Further to this, we may miss structures with interesting electronic properties. Therefore, our main objective is to find out a new phase of borophene, which is stable and semiconducting. However, unless we put a boundary, the possible combinations of structures are endless. For this, we have fixed the size of the supercell and created all possible defects. In this way, we have created some patterned defected structures, which match with previously reported systems. Then we have studied their energetics and compared with the previously reported systems. We find that such structures are energetically stable (based on total energy calculations) and they are not far (energetically) from the most stable structure. Therefore, uniform hole distribution is not an important criteria for their stability though they are more planar and metallic in nature. Therefore such structures may not be promising for semiconductor industries. Then we have tried to understand whether they (hole density, vacancy pattern, stability and electronic properties) have any relation between themselves. We find that the planarity and stability parameters have nothing to do with the low density at the Fermi level (i.e. energy balance position). Rather, an interplay between the hole density and hole distribution is crucial to get low density at the Fermi level. The low-coordinated sites around the holes may generate the energy balance position at the Fermi level as has been found in λ_5 sheet. More importantly, such defect engineering may be helpful to get the energy balance position in the high-energy phase structures. Below, we have presented the possibility of band gap opening at such energy balance position using strain.

3.4. Strain and Mechanical Stability:

3.4.1 Strain Induced Band Gap Opening:

The very interesting electronic property (very less electron density at the Fermi energy) of λ_5 (Figure 4f) sheet invokes our interest to study the electronic properties under strain. So, this particular pattern defect

creates a situation which is further helpful in opening of band gap by strain engineering. We have studied both compressive and tensile strain from 1% to 5% (Figure 5 and Figure S7-S16, Supporting Information) in both uniaxial and biaxial directions. For uniaxial direction, we have calculated through zigzag (along *a*) and straight (along *b*) direction (Figure 5a). Interestingly, we have found that band gap opening occurs in some cases under strain. We find that tensile strain opens the band gap only in biaxial and the uniaxial (along straight) directions (Figure 5b & 5c). Interestingly, compressive strain opens the band gap only in uniaxial (along zigzag) direction (Figure 5d). The band gap opening of the structures are in the range of 0.14 eV to 0.28 eV under the range of 1% to 5% biaxial strain (Table 2) with the maximum band gap opening under 3% applied strain (Figure 5b). The band gap opening for uniaxial tensile strain (along straight) is in the range of 0.16 eV to 0.28 eV under 1% to 5% strain (Table 2) with the maximum band gap opening at 3% applied strain (Figure 5c). The band gap opening for uniaxial compressive strain (zigzag direction) is in the range of 0.14 eV to 0.63 eV under 1% to 5% strain (Table 2) with the maximum band gap opening at 5% applied strain (Figure 5d). Therefore such λ_5 sheet is promising for electronic and optoelectronic applications.

Table 2: Band gap opening of λ_5 sheet under different % of applied strain calculated by HSE06 level of theory.

Types of Strain		**Band gap (eV)**				
		1%	**2%**	**3%**	**4%**	**5%**
Tensile	**Biaxial**	0.14	0.23	0.28	0.26	0.19
	Uniaxial (along-a)	No Gap	No Gap	No Gap	No Gap	No Gap
	Uniaxial (along-b)	0.16	0.28	0.28	0.26	0.26
Compressive	**Biaxial**	No Gap	No Gap	No Gap	No Gap	No Gap
	Uniaxial (along-a)	0.14	0.37	0.54	0.61	0.63
	Uniaxial (along-b)	No Gap	No Gap	No Gap	No Gap	No Gap

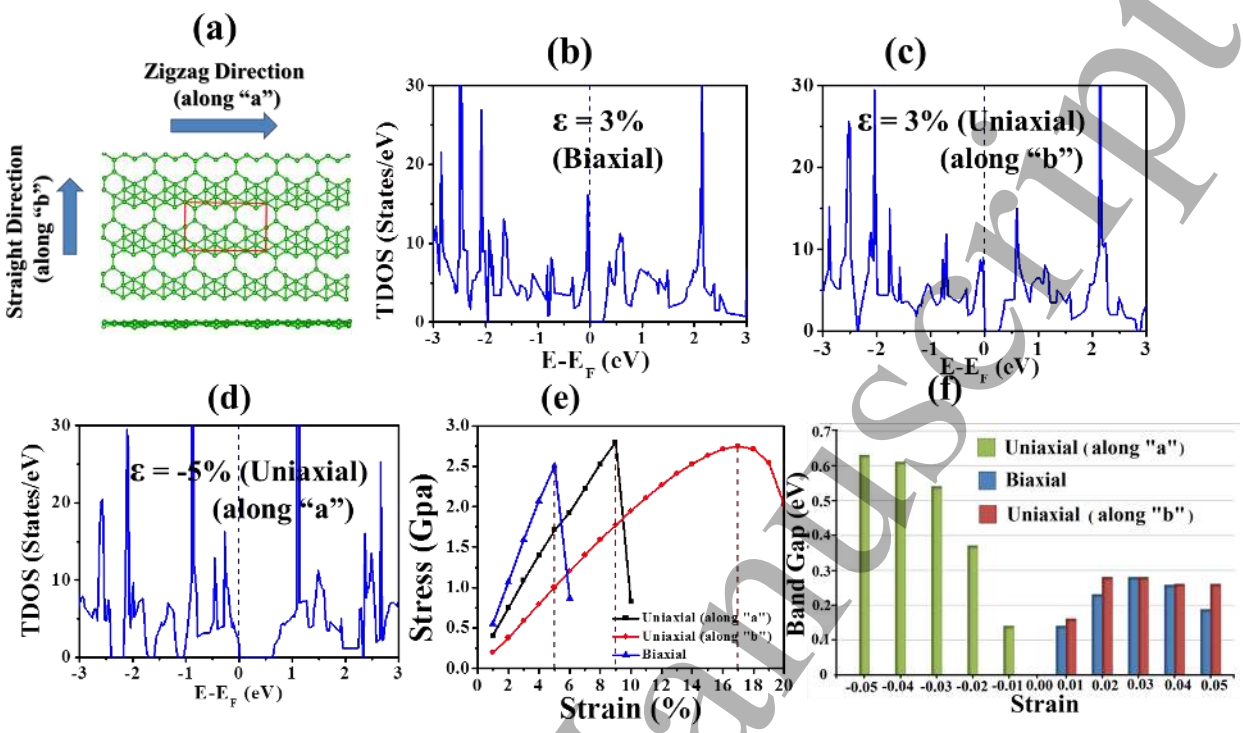

Figure 5: (a) structure of λ_5 sheet. The TDOS of λ_5 sheet under (b) 3% biaxial tensile, (c) 3% uniaxial tensile strain (along straight direction) and (d) 5% uniaxial compressive strain (along zigzag direction). (e) Strain vs. stress relationship for λ_5 sheet and the dotted lines indicate the elastic limit. (f) Graphical representation of variation of the band gap of λ_5 sheet under uniaxial and biaxial strains.

To check the reliability of our results, we have further performed the DOS analysis of λ_5 structure using PW91 and PBE0 functionals as has been shown in the Supporting Information (S17-S22). Here we presented the total density of states of biaxial tensile and uniaxial compressive strain along "a" and uniaxial tensile strain along "b" strain under 1, 2 and 3% strain.

We have found that the PW91 result matches with PBE calculation, without opening any band gap and possessing very low density at Fermi while strain is applied in biaxial way. In similar way, the band gap using PW91 is very much similar with PBE in case of uniaxial strain (along-a and along-b). Only uniaxial compressive strain at 5% strain along a opens a band gap of 0.08 eV in PW91 functional, whereas the system is band gap less in PBE functional. However in PBE0 calculation shows a band gap of 0.74 eV, 0.85 eV and 0.64 eV for 1%, 3% and 5% biaxial tensile strain, respectively. The band gaps are 0.71, 0.84

and 0.93 eV upon applying uniaxial tensile (along b direction) 1%, 3% and 5% strain, respectively. The band gaps are 0.93, 1.27 and 1.34 eV upon applying uniaxial compressive (along a direction) 1%, 3% and 5% strain, respectively. We have shown the comparative results in the table below (Table 3). Therefore, electronic properties do not change upon altering the GGA theory, whereas the PBE0 overestimates the band gap compared with HSE06. It is widely accepted that PBE0 overestimates the band gap compared to HSE06 calculation[57]. However, it is very interesting to find that semiconducting behavior of the strain induced λ_5 is irrespective with level of calculation.

Table 3: Band gap opening of λ_5 sheet under strain using different level of theories.

Strain		**Band Gap (eV)**			
		PW91	**PBE**	**HSE06**	**PBE0**
Biaxial Tensile	**1%**	0	0	0.14	0.74
	3%	0	0	0.28	0.85
	5%	0	0	0.19	0.64
Uniaxial Tensile (along b)	**1%**	0	0	0.16	0.71
	3%	0.09	0.05	0.28	0.84
	5%	0.11	0.12	0.26	0.93
Uniaxial Compressive (along a)	**1%**	0	0	0.14	0.93
	3%	0.13	0.12	0.54	1.27
	5%	0	0.08	0.63	1.34

We have also studied the possibility of band gap opening by applying 5% biaxial strain to other structures (α_2, λ_1 and λ_4), where the density of states near Fermi is less. We have found that none of cases opens a band gap. Below, we have shown the total density of states plot (using HSE06) of these systems (α_2, λ_1 and λ_4). We find that there is no band gap opening in these structures. Therefore, strain induced band gap opening is very much defect specific and thus, making λ_5 as a very unique pattern for band gap opening.

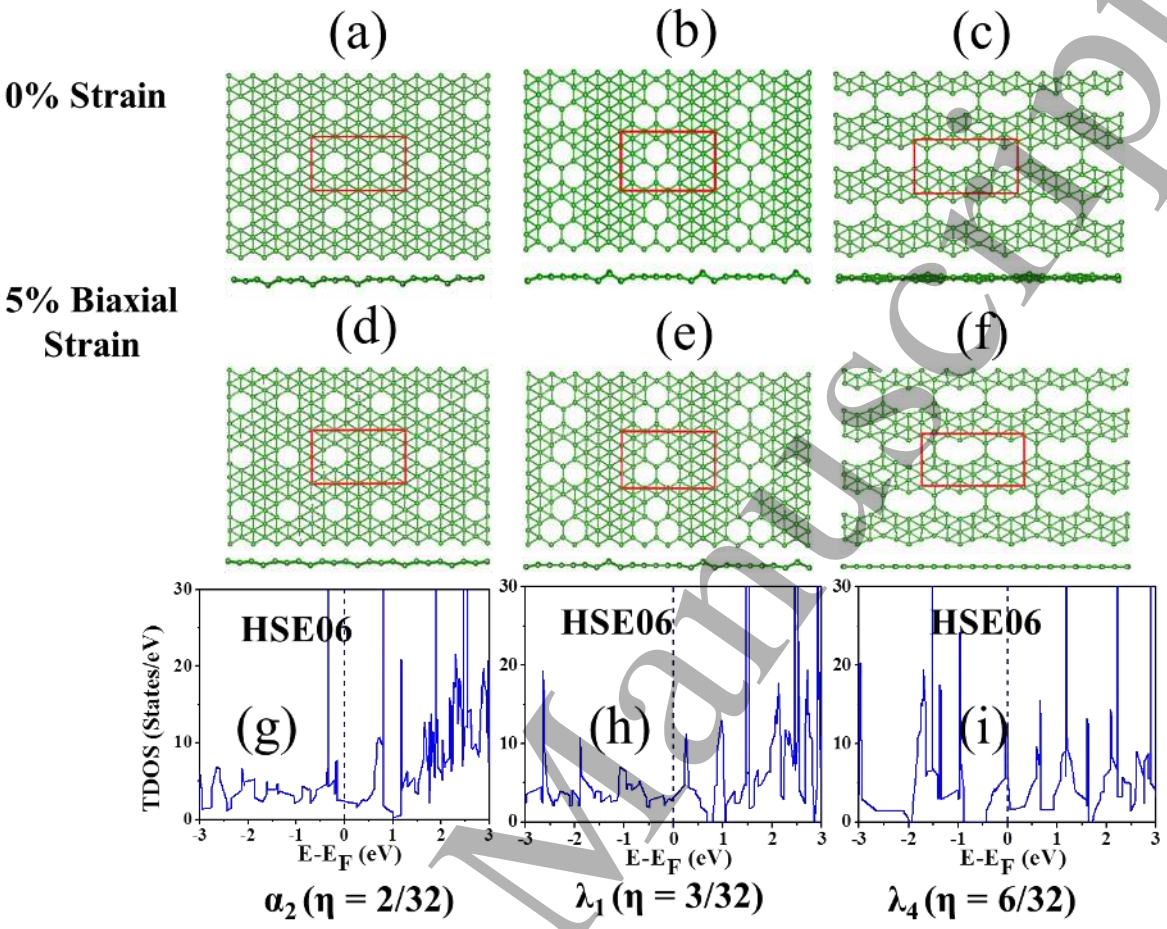

Figure 6: Structure of (a) α_2 sheet, (b) λ_1 sheet and (c) λ_4 sheet without application strain. Structure of (d) α_2 sheet, (e) λ_1 sheet and (f) λ_4 sheet with 5% biaxial tensile strain. The TDOS of (g) α_2 sheet, (h) λ_1 sheet and (i) λ_4 sheet under 5% biaxial tensile strain using HSE06 level of theory.

3.4.2 Mechanical Stability of λ_5:

Strain technology is crucial to evaluate and understand the fundamental nature of the chemical bonding, effect of lattice distortion on the structural stability and elastic limit of the single-layered system. Therefore, the λ_5 sheet should have enough structural stability to be isolated. Thus, it is crucial to assess the effect of structural distortion and mechanical stability under the strain for their synthesis and applications. Here, we have presented systematic analysis on the mechanical stability of λ_5 sheet,

including the ideal equi-biaxial tensile stress or equi-biaxial compressive stress and uniaxial tensile or compressive stress along direction "a" uniaxial tensile or compressive stress along direction "b". The % of applied strain is calculated using the formula as written below:[58]

$$\%\ of\ strain = \frac{a-a_1}{a} \times 100 \qquad (3)$$

Where 'a' and 'a_1' are the lattice constants of the boron monolayer sheet before and after the strain.

Tensile stress is applied along the in-plane uniaxial (both in zigzag and straight direction) and biaxial directions to evaluate the mechanical stability of λ_5 sheet. Atomic positions are relaxed at each strain until the forces on each atom are less than 10^{-3} eV $Å^{-1}$. Elastic limit is calculated from the stress-strain curve under the tensile strain (Figure 7b).[59] It shows that λ_5 sheet can sustain maximum equi-biaxial strain of 5%, maximum uniaxial strain of 9% along "a" (Zigzag direction) and maximum uniaxial strain of 17% along "b" (Straight direction). The critical strain along "a" direction is similar (8 %) with pure borophene sheet.[60] The elastic limit of λ_5 sheet is at 5% biaxial strain with a maximum stress of 2.5 GPa. Likewise, elastic limit of λ_5 sheet is at 9% uniaxial strain (along-a direction) with a maximum stress of 2.75 GPa and elastic limit is at 17% uniaxial strain (along-b direction) with a maximum stress of 2.75 GPa.

3.5 Dynamic Stability

The dynamic stability of various phases of borophene sheets have been analyzed from phonon frequency calculations. Phonon frequencies were calculated from phonon spectra, using the density functional perturbation theory (DFPT)[45] as implemented in VASP.[38] The lattice dynamics of λ_5 sheet is examined and compared with α-sheet from their respective phonon dispersion plots (Figure 7a-b). It has been found that alpha sheet has maximum negative frequency of 0.0013 THz. The λ_5 sheet has the negative frequency of 0.002 THz at Γ point and 2.55 THz at S point in the Brillouin zone. Furthermore, it has been reported[14] that phonon dispersion of freestanding borophene sheet contains small imaginary frequency near Γ point, which is consistent with instability against long-wavelength transverse wave. The authors have further suggested that this instability can be overcome by creating ripples or grain boundaries in the

crystals, which basically hinders the transverse waves by limiting the size of boron sheets. We have found that both pure borophene and α-sheet has been grown / synthesized[14,61] successfully on a substrate in spite of the small imaginary frequency in their phonon dispersion plot. It is reported that borophene and 2D polymorph of boron sheet are not stable in freestanding form. Mannix et al.[14] demonstrated that an atomically clean Ag (111) substrate provides the well-defined inert surface for borophene growth. Apart from pure borophene, the various phases of boron sheets with vacancy have also been grown on metal support. The experimental work by Feng et al.[16] showed that two dimensional boron sheets (β_{12} with η=1/6) and χ_3 with η=1/5) can be grown epitaxially on Ag (111) substrate. They have further mentioned that these sheets interact very weekly with their substrate.

Several theoretical studies also revealed that various phases of boron sheets with high hexagonal hole density can be synthesized on the support of metal surface. It is theoretically reported that a continuous growth of two-dimensional boron sheets ($g\text{-}_{2/15}$, $g\text{-}_{1/8}$, α, α_1, β_1) sheets with hole density 2/15,1/8,1/9, 1/8,1/7 on Cu(111) surface due to the low diffusion barrier for a single B atom on Cu (111) surface[61]. Using first-principles simulations, Yakobson's group [62] suggested that stable boron sheets with a certain density of hole can be derived by the deposition of B atoms on Au and Ag surface or saturation of B terminated MgB_2 surface in a B-rich environment. Furthermore, Karmodak et al.[50] calculated relative binding energy of various phases of boron sheets with different hole density on Ag (111) substrate. They have demonstrated that higher the hole density, lower the relative binding energy on Ag (111) substrate. Hence we can say that our λ_5 structure might possess lower binding energy on Ag(111) substrate. Therefore, based on these theoretical prediction and experimental validation of boron monolayer with hole density upto 0.2, we can predict that our structures also can be experimentally realizable on the support like Ag(111) and Cu(111).

We have also analyzed the negative frequency at r point and it has been found that these arise due to translation motion. Any non-trivial motion of atoms against each other is actual indication of unstable mode. But we have not found any such motion in our structure. Most of the boron based monolayers are

always grown on substrate since freestanding structures are not stable. Even, it has been found from the earlier published report[50] that any high energy phase (in freestanding calculation) became most stable while binding with substrate. This gives us an indication that our predicted structure may also be stable on substrate. Moreover, we have calculated phonon dispersion for all the phases of boron sheet (Figure S23 (a-q), Supporting Information) and we find that the structures hold negative phonon frequency in the range of -0.001 to -4.82 THz. Furthermore, we have studied the phonon dispersion for the semiconducting sheets (Figure S24 (a-c), Supporting Information) having imaginary frequency ranges 0.03 to 2.47 THz at Γ-point under 3% biaxial tensile strain, 3% uniaxial tensile strain (along "b") and 5% uniaxial compressive strain (along "a"). This suggests that these phases of borophene sheet may not be stable as a freestanding monolayer but can be synthesized on a substrate.

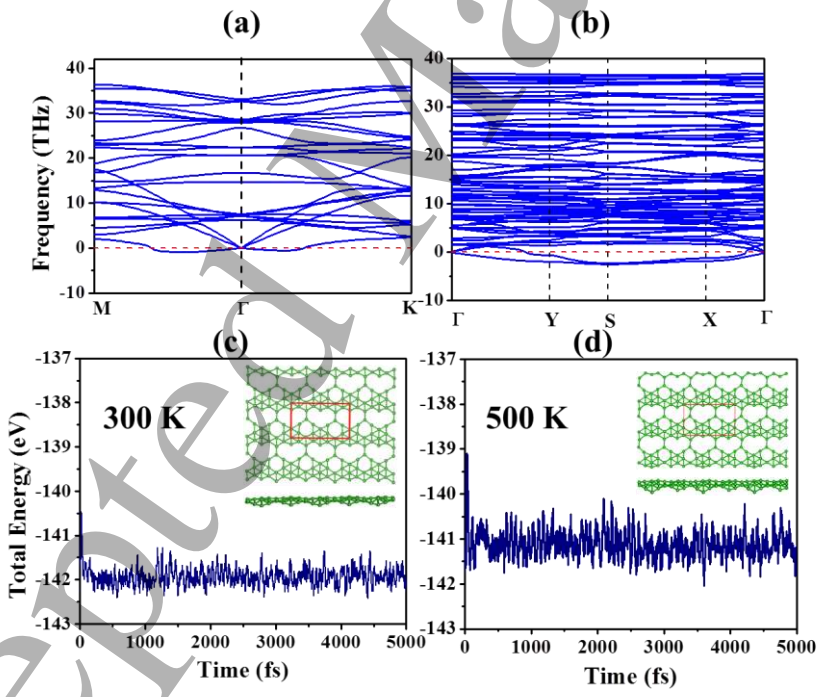

Figure 7: Phonon dispersion of (a) α-sheet and (b) λ_5 sheet. Total energy fluctuation during AIMD simulation of λ_5 sheet at (c) 300K and (d) 500K.

3.6 Thermal Stability

The thermal stability of the λ_5 sheet is studied by performing Ab initio molecular dynamics simulations (AIMD) using the Nosé thermostat model[47] as implemented in VASP.[38] Simulations are carried out using an NVT ensemble at 300 K, 500 K, and 1000 K with a time step of 1 fs for 5 ps. Room temperature AIMD simulation shows no possibility of inter-conversion from the optimized structure. No structural deformation has been observed for 300 and 500 K simulation (Figure 7c-d). However at 1000 K, the structure completely breaks (Figure S25, Supporting Information). Thus we predict that this structure is thermally stable though it might buckle and distorts at higher temperatures (1000 K).

We have done MD simulations up to 1000 K to check whether they have a very low energy barrier for converting into another structure or not. However, we find that the λ_5 structure does not convert into any other structure in the temperature range of 300-500 K. Furthermore, we have optimized the structures (Figure 7 and Figure S26 (a-c), Supporting Information)) after MD simulations. The MD-simulated structures show a buckling height of 0.90 and 0.93 Å for 300 and 500K, respectively compared to the DFT optimized structure (0.71 Å). It has been found that the optimized structures from DFT calculation are energetically comparable with the structure found from MD-simulated optimization at 300K and 500K.However at 1000K, MD-simulated optimized structure is more stable (by 4.21 eV) compared to DFT-optimized structure which might be due to the different pattern obtained after MD simulation.

4. Conclusion:

Using the density functional theoretical (DFT) calculations, we have demonstrated that hexagonal hole density and distribution of holes play important role in the stability and planarity of the various phases of boron sheets. We find that a system will show planarity only if the hole is evenly distributed over the sheet and the hole density fall in the range of $1/9 < \eta < 1/5$. In other cases, where the hole is not evenly distributed, it is extremely difficult to get a planar structure. Besides it is extremely difficult to explain the planarity/buckling of such structures based on the filled/vacant σ and π bands as the structure is neither perfectly buckled nor perfectly planar. Electronic properties of all the 17 different phases of boron sheets

are found to be metallic with hexagonal hole density ranging from 1/32 to 8/32. However, λ_5 sheet shows an interesting electronic property as it opens up band gap at the Fermi level under compressive/tensile strains. Moreover, dynamic stability of λ_5 sheet shows the existence of small imaginary frequency. Since such structures need to be grown on a metallic substrate for practical device applications, we expect that such small imaginary frequency will vanish when it will be growing on the substrate. Furthermore, we have accessed thermal and mechanical stabilities of λ_5 sheet to confirm the stability of the proposed structure. AIMD simulations confirmed that λ_5 sheet is a very stable sheet and can withstand temperature as high as 500 K. Moreover, the structure is stable under a considerable amount of strain. So, we predict that λ_5 sheet is a promising boron based material which can be very useful for device based applications.

5. Supporting Information:

The supporting information material is available free of charge on the website. Total and partial density of states (GGA-PBE and HSE06 level of theory) and phonon dispersion of different phases of borophene sheet with and without strain are given. Besides AIMD simulation (1000 K) of λ_5 sheet is given in supporting information.

6. Acknowledgement:

We thank IIT Indore for the lab and computing facilities. This work is supported by DST-SERB, (Project Number: EMR/2015/002057) New Delhi. G.B., A.M. and I.C. thank MHRD for research fellowships.

7. Reference:

[1] Gusynin V P , Sharapov S G 2006 Transport of Dirac quasiparticles in graphene: Hall and optical conductivities *Phys. Rev*. B **73** 245411

[2] Novoselov K S, Geim A K, Morozov S V, Jiang D, Katsnelson M I, Grigorieva I V, Dubonos S V, Firsov A A 2005 Two-dimensional gas of massless Dirac fermions in graphene *Nature* **438** 197–200

[3] Pang S P, Hernandez Y, Feng X L, Mullen K 2011 Graphene as Transparent Electrode Material for Organic Electronics *Adv. Mater.* **23** 2779–2795

[4] Gomez-Navarro C, Burghard M, Kern K 2008 Elastic Properties of Chemically Derived Single Graphene Sheets *Nano Lett.* **8** 2045–2049.

[5] Calizo I, Balandin A A, Bao W, Miao F, Lau C N 2007 Temperature Dependence of the Raman Spectra of Graphene and Graphene Multilayers *Nano Lett.* **7** 2645–2649

[6] Lin Y M, Dimitrakopoulos C, Jenkins, K A, Farmer D B, Chiu H Y, Grill A, Avouris P 2010 100-GHz Transistors from Wafer-Scale Epitaxial Graphene *Science* **327** 662– 662

[7] Bae S, Kim H, Lee Y, Xu X F, Park J S, Zheng Y, Balakrishnan J, Lei T, Kim H R, Song Y I, Kim Y J, Kim K S, Ozyilmaz B, Ahn J H, Hong B H, Iijima S 2010 Roll-to-roll production of 30-inch graphene films for transparent electrodes *Nat. Nanotechnol.* **5** 574–578

[8] Liu M, Yin X B, Ulin-Avila E, Geng B S, Zentgraf T, Ju L, Wang F, Zhang X 2011 A graphene-based broadband optical modulator *Nature* **474** 64–67

[9] Robinson J T, Perkins F K, Snow E S, Wei Z Q, Sheehan P E 2008 Reduced Graphene Oxide Molecular Sensors *Nano Lett.* **8** 3137–3140

[10] Kim K S, Zhao Y, Jang H, Lee S Y, Kim J M, Ahn J H, Kim P, Choi J Y, Hong B H 2009 Large-scale pattern growth of graphene films for stretchable transparent electrodes *Nature* **457** 706–710

[11] Wu H, Qian Y, Lu S, Kan E, Lu R, Deng K, Wanga H, Ma Y 2015 Two-dimensional silicon monolayers generated on c-BN(111) substrate *Phys. Chem. Chem. Phys.* **17** 15694

[12] Dávila M E, Lay G L 2016 Few layer epitaxial germanene: a novel two-dimensional Dirac material *Sci. Rep.* **6** 20714

[13] Zhu F F, Chen W J, Xu Y, Gao C L, Guan D D, Liu C H, Qian D, Zhang S C, Jia J F 2015 Epitaxial growth of two-dimensional stanene *Nat. Mater.* **14** 1020-1025

[14] Mannix A J, Zhou X F, Kiraly B, Wood J D, Alducin D, Myers B D, Liu X, Fisher B L, Santiago U, Guest J R, Yacaman M J, Ponce A, Oganov A R, Hersam M C, Guisinger N P 2015 Synthesis of borophenes: Anisotropic, two-dimensional boron polymorphs *Science* **350** 1513-1516

[15] Liu X, Wei Z, Balla I, Mannix A J, Guisinger N P, Luijten E, Hersam M C 2017 Self-assembly of electronically abrupt borophene/organic lateral heterostructures *Sci. Adv.* **3** 1602356

[16] Feng B, Zhang J, Zhong Q, Li W, Li S, Li H, Cheng P, Meng S, Chen L, Wu K 2016 Experimental realization of two-dimensional boron sheets *Nat. Chem.* **8** 563-568

[17] Woomer A H, Farnsworth T W, Hu J, Wells R A, Donley C L, Warren S C 2015 Phosphorene: Synthesis, Scale-Up, and Quantitative Optical Spectroscopy *ACS Nano.* **9** 8869–8884

[18] Ozdogan C, Mukhopadhyay S, Hayami W, Güvenc Z B, Pandey R, Boustani I 2010 The Unusually Stable B100 Fullerene, Structural Transitions in Boron Nanostructures, and a Comparative Study of α- and γ-Boron and Sheets *J. Phys. Chem.* C **114** 4362–4375

[19] Ciuparu D, Klie R F, Zhu Y, Pfefferle L 2004 Synthesis of Pure Boron Single-Wall Nanotubes *J. Phys. Chem.* B 108 3967-3969

[20] Liu F, Shen C, Su Z, Ding X, Deng S, Chen J, Xu N, Gao H 2010 Metal-like single crystalline boron nanotubes: synthesis and in situ study on electric transport and field emission properties *J. Mater. Chem.* 20 2197

[21] Li X B, Xie S Y, Zheng H, Quan Tianc W, Sun H B 2015 Boron based two-dimensional crystals: theoretical design, realization proposal and applications *Nanoscale* **7** 18863

[22] Ugeda M M, Brihuega I, Hiebel F, Mallet P, Veuillen J Y, Gomez-Rodrıguez J M, Yndurain F 2012 Electronic and structural characterization of divacancies in irradiated graphene *Phys. Rev.* B **85** 121402

[23] Lusk M T, Carr L D 2008 Nanoengineering Defect Structures on Graphene *Phys. Rev. Lett.* **100** 175503

[24] Zhu T, Ertekin E 2016 Generalized Debye-Peierls/Allen-Feldman model for the lattice thermal conductivity of low-dimensional and disordered materials *Phys. Rev. B* **93** 155414

[25] Zhu T, Ertekin E 2016 Phonons, Localization, and Thermal Conductivity of Diamond Nanothreads and Amorphous Graphene *Nano Lett.* **16** 4763−4772

[26] Pedersen T G, Flindt C, Pedersen J, Mortensen N A, Jauho Antti-Pekka, Pedersen K 2008 Graphene Antidot Lattices: Designed Defects and Spin Qubits *Phys. Rev. Lett.* **100** 136804

[27] Tang H, Ismail-Beigi S 2007 Novel Precursors for Boron Nanotubes: The Competition of Two-Center and Three-Center Bonding in Boron Sheets *Phys. Rev. Lett.* **99** 115501

[28] Wu X, Dai J, Zhao Y, Zhuo Z , Yang J, Zen X C 2012 Two-Dimensional Boron Monolayer Sheets *ACS Nano*. 6 7443–7453

[29] Lu H, Mu Y, Bai H, Chen Q, Li S D 2013 Binary nature of monolayer boron sheets from ab initio global searches *J. Chem. Phys.* **138** 024701

[30] Penev E S, Bhowmick S, Sadrzadeh A, Yakobson B I 2012 Polymorphism of Two-Dimensional Boron *Nano Lett.* **12** 2441-2445.

[31] Penev E S, Kutana A, Yakobson B I 2016 Can Two-Dimensional Boron Superconduct? *Nano Lett.* **16** 2522−2526

[32] Li X, Dai Y, Ma Y, Han S, Huang B 2014 Graphene/g-C3N4 bilayer: considerable band gap opening and effective band structure engineering *Phys. Chem. Chem. Phys.* **16** 4230-4235

[33] Son Y W, Cohen M L, Louie S G 2006 Energy gaps in graphene nanoribbons *Phys. Rev. Lett.* **97** 216803

[34] Yan J A, Xian L, Chou M Y 2009 Structural and electronic properties of oxidized graphene *Phys. Rev. Lett.* **103** 086802

[35] Garg P, Choudhuri I, Mahata A, Pathak B 2017 Band gap opening in stanene induced by patterned B–N doping *Phys. Chem. Chem. Phys.* **19** 3660-3669

[36] Dvorak M, Oswald W, Wu Z, 2013 Bandgap Opening by Patterning Graphene *Sci. Rep.* **3** 2289

[37] Guinea F, Katsnelson M, Geim A 2009 Energy gaps and a zero-field quantum Hall effect in graphene by strain engineering *Nat. Phys.* **6** 30

[38] Kresse G, Furthmuller J 1996 Efficient Iterative Schemes for ab initio Total-energy Calculations using a Plane-wave Basis Set *Phys. Rev. B: Condens. Matter Mater. Phys.* **54** 11169−11186

[39] Perdew J P, Burke K, Ernzerhof M 1996 Generalized Gradient Approximation Made Simple *Phys. Rev. Lett.* **77** 3865−3868

[40] Perdew J P, Chevary J A, Vosko S H, Fiolhais C 1992 Atoms, Molecules, Solids, and Surfaces: Applications of the Generalized Gradient Approximation for Exchange and Correlation *Phys. Rev. B: Condens. Matter Mater. Phys.* **46** 6671−6687

[41] Blochl P E 1994 Projector Augmented Wave Method *Phys. Rev. B: Condens. Matter Mater. Phys.* 50 17953−17979

[42] Sham L J, Schlüter M 1983 Density-Functional Theory of the Energy Gap *Phys. Rev. Lett.* **51** 1888–1891

[43] Mori-Sánchez P, Cohen A J, Yang W 2008 Localization and Delocalization Errors in Density Functional Theory and Implications for Band-Gap Prediction *Phys. Rev. Lett.* 100 146401

[44] Heyd J, Scuseria G E, Ernzerhof M 2003 Hybrid Functionals Based on a Screened Coulomb Potential *J. Chem. Phys.* **118** 8207−8215

[45] Baroni S, Giannozzi P, Testa A 1987 Green's-function approach to linear response in solids *Phys. Rev. Lett.* **58** 1861–1864

[46] Zhang S, Zhou J, Wang Q, Chen X, Kawazoe Y, Jena P 2015 Penta-graphene: A new carbon allotrope *Proc. Natl. Acad. Sci. U. S. A.* **112** 2372–2377

[47] Nosé S 1984 A Unified Formulation of the Constant Temperature Molecular Dynamics Methods *J. Chem. Phys.* **81** 511−519

[48] Hummer K, Har J, Kresse G 2009 Heyd-Scuseria-Ernzerhof hybrid functional for calculating the lattice dynamics of semiconductors *Phys. Rev. B* **80** 115205

[49] Choudhuri I, Bhattacharyya G, Kumar S, Pathak B 2016 Metal-Free Half-Metallicity in a High Energy Phase C-doped gh-C3N4 System: A High Curie Temperature Planar System *J. Mater. Chem. C* **4** 11530-11539

[50] Karmodak N, Jemmis E D 2017 The Role of Holes in Borophenes: An Ab Initio Study of Their Structure and Stability with and without Metal Templates *Angew. Chem. Int. Ed.* DOI: 10.1002/anie.201610584

[51] Tang H, Ismail-Beigi S 2010 First-Principles Study of Boron Sheets and Nanotubes *Phys. Rev.* B **82** 115412

[52] Choudhuri I, Pathak B 2017 Ferromagnetism and Half-metallicity in Atomically Thin Holey Nitrogenated Graphene Based System ChemPhysChem DOI: 10.1002/cphc.201700633

[53] Boustani I 1997 Systematic ab initio investigation of bare boron clusters: Determination of the geometry and electronic structures of Bn (n=2 – 14) *Phys. Rev.* B **55** 16426

[54] Wang Z, Lu T Y, Wang H Q, Feng Y P, Zheng J C 2016 High anisotropy of fully hydrogenated borophene *Phys. Chem. Chem. Phys.* **18** 31424—31430

[55] Peng B, Zhang H, Shao H, Xu Y, Zhang R, Zhua H 2016 The electronic, optical, and thermodynamic properties of borophene from first-principles calculations *J. Mater. Chem.* C **4** 3592-3598

[56] Xie S Y, Li X B, Tian W Q, Chen N K, Wang Y, Zhang S, Sun H B 2015 A novel two-dimensional MgB6 crystal: metal-layer stabilized boron kagome lattice *Phys. Chem. Chem. Phys.* **17** 1093-1098

[57] Garza A J, Scuseria G E 2016 Predicting Band Gaps with Hybrid Density Functionals *J. Phys. Chem. Lett.* **7** 4165−4170

[58] Topsakal M, Ciracil S 2010 Elastic and Plastic Deformation of Graphene, Silicene, and Boron Nitride Honeycomb Nanoribbons under Uniaxial Tension: A First-principles Density-functional Theory Study *Phys. Rev. B: Condens. Matter Mater. Phys.* **81** 024107

[59] Nisar J, Jiang X, Pathak B, Zhao J, Kang T W, Ahuja R 2012 Semiconducting Allotrope of Graphene *Nanotechnology* **23** 385704

[60] Haifeng W, Li Q, Gao Y, Miao F, X Zhou F, X. Wan, G 2016 Strain effects on borophene: ideal strength, negative Possion's ratio and phonon instability *New J. Phys.* **18** 073016

[61] Liu H, Gao J, Zhao J 2013 From Boron Cluster to Two-Dimensional Boron Sheet on Cu(111) Surface: Growth Mechanism and Hole Formation *Sci. Rep.* **3** 3238

[62] Liu Y, Penev E S, Yakobson B I 2013 Probing the synthesis of two-dimensional boron by first-principles computations. *Angew. Chem.* **52**, 3238–3241.